Distributed Parameter Modelling and Finite-Frequency Loop-Shaping of Electromagnetic Molding Machine

Takayuki Ishizaki[a], Kenji Kashima[b], Jun-ichi Imura[a], Atsushi Katoh[c], Hiroshi Morita[c], Kazuyuki Aihara[d]

[a]*Graduate School of Information Science and Engineering, Tokyo Institute of Technology; 2-12-1, Meguro, Tokyo, Japan*
[b]*Graduate School of Engineering Science, Osaka University; 1-3, Machikaneyama, Toyonaka, Osaka, Japan*
[c]*Sumitomo Heavy Industries, Ltd; 19, Natsushima, Yokosuka, Kanagawa, Japan*
[d]*Institute of Industrial Science, University of Tokyo 4-6-1, Komaba, Meguro ward, Tokyo, Japan*

Abstract

We derive a mathematical model for an electromagnet inside a molding machine, and propose a novel loop-shaping method of the proportional-integral (PI) controller design for the system based on the generalized KYP (GKYP) lemma. The behavior of the molding machine is difficult to capture by using finite-dimensional models owing to eddy currents spatially distributed throughout the electromagnet. To analyze fundamental properties of the system both theoretically and experimentally, we first derive a mathematical model of the machine in terms of a partial differential equation (PDE). An analysis using the PDE model shows that a low-dimensional approximation performed by standard spatial discretization results in a spillover effect, which makes the behavior of the closed-loop system oscillatory. Then, to develop an easily tunable and implementable control system, we propose a novel loop-shaping method for PI control on the basis of the GKYP lemma. In this control system design, we use multiple low-dimensional models, which work simultaneously in specified finite frequency ranges. The proposed method successfully suppresses the spillover effect despite the use of low-dimensional approximants. Finally, we show the efficiency of the proposed control design method through numerical and experimental verification and discuss a performance limitation of the PI control.

Keywords: Industrial applications of optimal control, Modeling for control optimization, Infinite-dimensional systems, Generalized KYP lemma, Electromagnet.

1. Introduction

In recent molding processes, molding machines driven by hydraulic power have been gradually replaced with ones driven by electric power to improve control performance as well as job cycling time. Against this background, a novel molding machine driven by electromagnetic power has recently been developed in (Morita et al., 2009). The machine's clear contrast to ordinary ones is that the driving force generated by the electromagnets is directly transmitted to a mold without an amplifier. This kind of direct mold drive has the potential to carry out more precise molding fabrication than traditional machines.

To fully utilize the hardware improvement of the molding machine, we should also develop a control system that can be implemented into practical industrial instruments. As one traditional control method, the frequency response method has remained eminent in industrial applications (DiStefano et al., 1997; Friedland, 2012), and has helped control engineers improve the performance of feedback control system as well as understand how feedback control works. Along

with the frequency response method, proportional-integral-derivative (PID) based control is still the most commonly used technique for current industrial applications (Astrom and Hagglund, 1995; O'Dwyer, 2009), although modern control theory has made great progress in the past few decades; see (Brogan, 1990; Zhiqiang and Rhinehart, 2004) for an overview. This gap between theory and practice could be caused by hesitation among manufacturers to implement major refurbishment of existing equipment. In industry, such refurbishment is time-consuming and often requires considerable operator training costs. In view of this, aiming at industrial application, we should explicitly take into account that

- the control system to be designed can be implemented into the existing environment, and

- the design specification (optimization criterion) is simply adjustable by engineers and operators.

To comply with such industrial requirements, in this paper we focus on designing a PI control system that is compatible with practical equipment. A number of PI controller tuning techniques are available for controller design (Astrom and Hagglund, 1995; O'Dwyer, 2009). However, an experiment shown in this paper suggests that standard tuning techniques, such as the Ziegler-Nichols tuning rule (Astrom and Hagglund, 1995), do not work well for our electromagnetic molding ma-

chine. This is because eddy currents, which are spatially distributed within the electromagnet, cause unexpected behavior of the feedback control system. To properly handle these spatially distributed eddy currents, the dynamics of the electromagnet should be modeled as a distributed parameter system (Curtain and Zwart, 1995; Crank, 1973; Deen, 1998); see Section 2 for details.

For various kinds of distributed parameter systems, optimal control problems have been addressed in much of the literature (e.g., Curtain and Zwart, 1995; Padhi and Ali, 2009; Li and Christofides, 2008; Becker and Vexler, 2007; Calise et al., 1990). However, since most of these controllers are infinite-dimensional (or relatively high-dimensional), they are not easily implementable.

As another possible approach, model reduction-based control synthesis methods have also been developed; see (e.g., Li and Qi, 2010; Zheng et al., 2002). However, it is well known that a low-dimensional approximation of distributed parameter systems often results in undesirable behavior in the feedback control system owing to the negative influence of the unmodeled (ignored) dynamics. This phenomenon is called a spillover effect (Balas, 1978; Lin, 1981; Bontsema and Curtain, 1988).

In contrast to these approaches, in this paper we develop a novel PI control design method for an electromagnetic molding machine. We first derive its system expression in terms of a partial differential equation (PDE) according to the basic laws of physics. Then we analyze the fundamental system properties both theoretically and experimentally. This system analysis shows that a low-dimensional approximation via standard spatial discretization causes the aforementioned spillover effect in the feedback control system. In view of this, we propose a novel finite-frequency loop-shaping method based on the generalized KYP (GKYP) lemma (Iwasaki and Hara, 2005; Hara et al., 2006). In the proposed method, we introduce multiple low-dimensional models that work in specified finite frequency ranges. It is experimentally demonstrated that the method successfully suppresses the spillover effect despite using a low-dimensional approximation. The effectiveness of the proposed method is shown through numerical and experimental verification, and a performance limit of the PI control is briefly discussed at the end of this paper.

This paper is organized as follows: In Section 2 we overview the electromagnetic molding machine dealt with in this paper. Next, in Section 3, we derive a PDE that expresses its system behavior, and we analyze its fundamental system properties. By using the PDE expression, we show that a low-dimensional approximation performed by the ordinary spatial discretization results in a spillover effect. In Section 4 we propose a novel finite-frequency loop-shaping method for the PI control system design, and in Section 5 show the efficacy of the proposed method through numerical and experimental verification. Finally, concluding remarks are provided in Section 6.

2. Overview of the Electromagnetic Molding Machine

In this section, we overview the electromagnetic molding machine dealt with in this paper. The photograph of a pro-
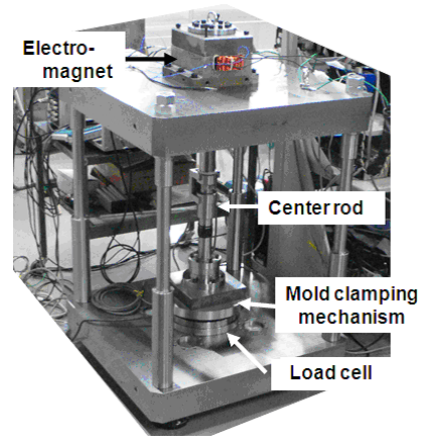
Figure 1: Prototype System.
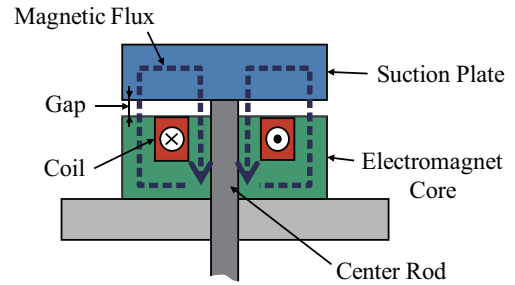
Figure 2: Depiction of Electromagnet.

totype system is shown in Fig. 1. This system consists of an *electromagnet* for generating a molding force, a *center rod* for transmitting the generated force, and a *clamping mechanism* for performing molding. The mold clamping mechanism includes a *load cell*, for observing the molding force. Figure 2 depicts the electromagnet placed inside the system, which is composed of an *electromagnet core*, a *suction plate* and a *coil*. This electromagnet produces suction force at *gaps* between the electromagnet core and the suction plate. The suction force is transmitted to the mold inside the clamping mechanism through the center rod.

To achieve fast and precise molding, it is desirable that the force response settles in a short time without overshoot. Figure 3 shows a block diagram of our PI control equipment. In this control system, a low-pass filter is embedded to reduce high-frequency output noise. This filter can be regarded as part of the plant dynamics; see Section 4.2 for its explicit characteristics. The experimental results for a step response are shown in Figure 4, where the value of the proportional gain is varied from 0.005 to 0.1, while the value of the integral gain is fixed at 0.01. The figure shows that the response becomes more oscillatory as we increase the proportional gain. It is well known that this kind of the oscillatory behavior appears in traditional gain tuning (e.g., Astrom and Hagglund, 1995; O'Dwyer, 2009). The figure further shows that the response takes considerable time to settle to its steady-state value (~0.05 s). Such poor settling
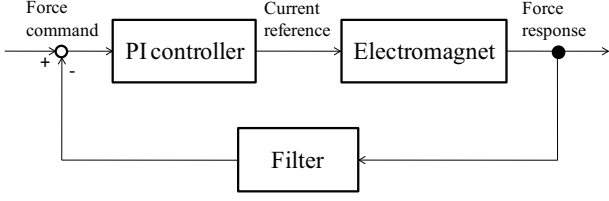
Figure 3: PI Control System.
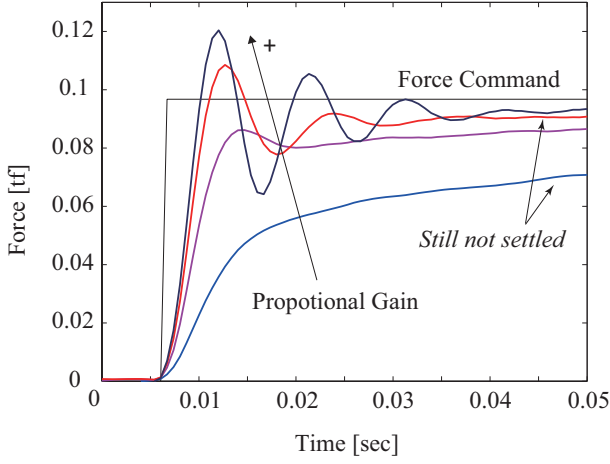
Figure 4: Step Response of the Electromagnetic Molding Machine.

time possibly spoils the reliability of the traditional parameter tuning strategies, e.g., the Ziegler-Nichols tuning rule, because they explicitly use a set of constants determined from the step response, such as steady-state value and transient rate, to decide the PI gain parameters. In view of this, we need to develop a gain determination method to systematically improve the machine response.

3. Distributed Parameter Modelling and Fundamental Analysis

In this section, to analyze system properties theoretically, we derive a mathematical model of the electromagnet. In what follows, according to the basic laws of physics (Cheng, 1992), we investigate a relation between the input current u in the coil and the output suction force F_{out} generated by magnetic flux.

As shown in Fig. 5, where a cross section of the electromagnet is depicted, the physics is supposed to be axisymmetric. According to the symmetry, we consider a micro region $\mathcal{D}$ along the path of an eddy current i_e at a radial position r. First, the suction force F_{out} is given by

$$F_{\text{out}}(t) = \frac{1}{2\mu_0} \int_0^{r_{\max}} B^2(t,r) 2\pi r dr \qquad (1)$$

where μ_0 denotes the magnetic permeability in vacuum, $r_{\max}$ denotes the radius of the iron core, and B denotes the density of magnetic flux. We consider (1) as an output equation with
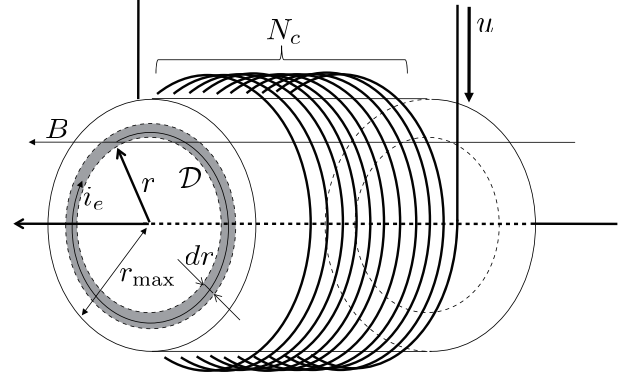
Figure 5: Electromagnet Model.

respect to the state variable of B. Here, the magnetic flux is given by

$$B(t,r) = \frac{E_M(t,r)}{R_M(r) 2\pi r dr}$$

where E_M denotes the magnetomotive force induced by the currents u and i_e, and R_M denotes the magnetic resistance of the iron core. The magnetic resistance is expressed as

$$R_M(r) = \frac{\sigma}{2\pi r}, \quad \sigma := \left(\frac{L}{\mu_0 \mu_s} + \frac{d}{\mu_0} \right)$$

where L denotes the length of the iron core, μ_s the relative magnetic permeability, and d the gap distance in the electromagnet.

Next, we derive an expression of the magnetomotive force E_M. A resistance R_E of the iron core, which is proportional to the circumferential length and inversely proportional to the width of the path, is given by

$$R_E(r) = \frac{2\pi r}{dr} \rho$$

where ρ denotes a material constant of the iron core. Thus the eddy current i_e in $\mathcal{D}$ is obtained as

$$i_e(t,r) = \frac{E_E(t,r)}{R_E(r)} = \frac{E_E(t,r)}{2\pi r \rho} dr$$

where E_E denotes the electromotive force induced by B. From Faraday's law of electromagnetic induction, E_E is expressed by

$$E_E(t,r) = - \int_0^r 2\pi \zeta \frac{\partial B(t,\zeta)}{\partial t} d\zeta.$$

Since E_M is given by the sum of magnetomotive forces outside $\mathcal{D}$, we obtain

$$E_M(t,r) = \frac{dr}{r_{\max}} N_c u(t) - \frac{dr}{\rho} \int_r^{r_{\max}} \frac{1}{\zeta'} \int_0^{\zeta'} \zeta \frac{\partial B(t,\zeta)}{\partial t} d\zeta d\zeta'$$

where N_c denotes the number of coil turns. The above equations lead to the state equation

$$B(t,r) = \frac{N_c}{\sigma r_{\max}} u(t) - \frac{1}{\sigma \rho} \int_r^{r_{\max}} \frac{1}{\zeta'} \int_0^{\zeta'} \zeta \frac{\partial B(t,\zeta)}{\partial t} d\zeta d\zeta'. \qquad (2)$$

3

Finally, differentiating both sides of (2) with respect to r and linearizing (1) around an operating point $(\overline{u}, \overline{B}, \overline{F}_{\text{out}})$ of the system, we obtain the linearized state-space representation as

$$
\begin{cases}
\dfrac{\partial X(t,\xi)}{\partial t} = 2\alpha \dfrac{\partial}{\partial \xi}\left(\xi \dfrac{\partial X(t,\xi)}{\partial \xi}\right), & \xi \in (0,1) \\[2mm]
X(t,\xi) = \dfrac{\beta}{\alpha} u(t), & \xi = 1 \\[2mm]
\xi \dfrac{\partial X(t,\xi)}{\partial \xi} = 0, & \xi = 0 \\[2mm]
y(t) = \displaystyle\int_0^1 X(t,\xi)\,d\xi
\end{cases}
\tag{3}
$$

where

$$
\xi := \left(\frac{r}{r_{\max}}\right)^2, \quad X(t,\xi) := B\left(t,\sqrt{\xi}\right),
$$

$$
\alpha := \frac{2\sigma\rho}{r_{\max}^2}, \qquad \beta := \frac{2\pi\rho N_c^2 \overline{F}_{\text{out}}}{\sigma\mu_0}.
$$

The modelling error resulting from the linearization could be significant if we run the machine far away from the operating point. In view of this, all experiments shown in the following are performed close to the operating point so that the linearization is reasonable enough. We can see from (3) that the system dynamics is essentially identical to that of spatially one-dimensional thermal diffusion systems with diffusivity proportional to the spatial variable (see, e.g., Crank, 1973; Deen, 1998; Carslaw and Jaeger, 1986, for an overview of diffusion systems). Based on this representation, we obtain the input-to-output characteristics in the Laplace domain as follows:

Theorem 1. *The transfer function of (3) from u to y is given by*

$$
G_\infty(s) := \frac{\beta}{\alpha} \frac{J_1\left(2\sqrt{-\frac{s}{2\alpha}}\right)}{\sqrt{-\frac{s}{2\alpha}}\, J_0\left(2\sqrt{-\frac{s}{2\alpha}}\right)}
\tag{4}
$$

where

$$
J_k(z) := \sum_{m=0}^\infty \frac{(-1)^m}{m!\,(m+k)!}\left(\frac{z}{2}\right)^{2m+k}, \quad k \in \{1,2\}.
\tag{5}
$$

Proof. We prove the claim by following the procedure of transfer function derivation (Curtain and Zwart, 1995; Curtain and Morris, 2009). From the Laplace transform of (3) with respect to t, we have

$$
\begin{cases}
sX(s,\xi) = 2\alpha \dfrac{\partial}{\partial \xi}\left(\xi \dfrac{\partial X(s,\xi)}{\partial \xi}\right), & \xi \in (0,1) \\[2mm]
X(s,\xi) = \dfrac{\beta}{\alpha} U(s), & \xi = 1 \\[2mm]
\xi \dfrac{\partial X(s,\xi)}{\partial \xi} = 0, & \xi = 0 \\[2mm]
Y(s) = \displaystyle\int_0^1 X(s,\xi)\,d\xi
\end{cases}
\tag{6}
$$

where X, U and Y denote the Laplace transform of X, u and y, respectively. We show that the solution of the two-point boundary value problem in (6) is given by

$$
X(s,\xi) = \frac{\beta}{\alpha} \frac{J_0\left(2\sqrt{-\frac{s}{2\alpha}}\right)}{J_0\left(2\sqrt{-\frac{s}{2\alpha}}\right)} U(s).
\tag{7}
$$

Note that (7) is expressed by

$$
X(s,\xi) = \frac{\beta}{\alpha} \frac{\sum_{m=0}^\infty \frac{1}{(m!)^2}\left(\frac{s\xi}{2\alpha}\right)^m}{\sum_{m=0}^\infty \frac{1}{(m!)^2}\left(\frac{s}{2\alpha}\right)^m} U(s)
\tag{8}
$$

from the definition of J_k, which is known as the Bessel function (McLachlan, 1955). Substituting (8) into the first equation of (6) yields

$$
\begin{aligned}
\text{(LHS)} &= \frac{\beta}{\alpha} \frac{\sum_{m=0}^\infty \frac{1}{(m!)^2}\left(\frac{\xi}{2\alpha}\right)^m s^{m+1}}{\sum_{m=0}^\infty \frac{1}{(m!)^2}\left(\frac{s}{2\alpha}\right)^m} U(s) \\[2mm]
\text{(RHS)} &= 2\alpha \frac{\partial}{\partial \xi}\left\{ \xi \frac{\beta}{\alpha} \frac{\sum_{m=1}^\infty \frac{m}{(m!)^2}\left(\frac{s}{2\alpha}\right)^m \xi^{m-1}}{\sum_{m=0}^\infty \frac{1}{(m!)^2}\left(\frac{s}{2\alpha}\right)^m} U(s) \right\} \\[2mm]
&= 2\alpha \frac{\beta}{\alpha} \frac{\sum_{m=1}^\infty \frac{1}{\{(m-1)!\}^2}\left(\frac{s}{2\alpha}\right)^m \xi^{m-1}}{\sum_{m=0}^\infty \frac{1}{(m!)^2}\left(\frac{s}{2\alpha}\right)^m} U(s) \\[2mm]
&= \frac{\beta}{\alpha} \frac{\sum_{m'=0}^\infty \frac{1}{(m'!)^2}\left(\frac{\xi}{2\alpha}\right)^{m'} s^{m'+1}}{\sum_{m=0}^\infty \frac{1}{(m!)^2}\left(\frac{s}{2\alpha}\right)^m} U(s)
\end{aligned}
$$

where $m' := m - 1$. Note that (7) also satisfies the second and third boundary conditions. Finally, from

$$
\begin{aligned}
\int_0^1 J_0\left(2\sqrt{-\frac{s\xi}{2\alpha}}\right)d\xi &= \int_0^1 \sum_{m=0}^\infty \frac{1}{(m!)^2}\left(\frac{s\xi}{2\alpha}\right)^m d\xi \\[2mm]
&= \sum_{m=0}^\infty \frac{1}{m!\,(m+1)!}\left(\frac{s}{2\alpha}\right)^m \\[2mm]
&= \left(\sqrt{-\frac{s}{2\alpha}}\right)^{-1} J_1\left(2\sqrt{-\frac{s}{2\alpha}}\right),
\end{aligned}
$$

the result follows. $\qquad\square$

This theorem shows that the input-to-output characteristics have an explicit expression in terms of the Bessel function. Furthermore, the following theorem describes particular properties of G_∞:

Theorem 2. *The transfer function G_∞ in (4) satisfies the following:*

(i) *It is an $\mathcal{H}_\infty$-function expressed as the ratio of entire functions.*

(ii) *The zeros and poles of G_∞ are all negative real numbers, and they interlace with each other.*

(iii) *The high- and low-frequency properties of G_∞ are given by*

$$
\begin{cases}
G_\infty(0) = \dfrac{\beta}{\alpha} \\[3mm]
G_\infty(j\omega) \sim \dfrac{\beta}{\alpha}\sqrt{\dfrac{2\alpha}{j\omega}}, & \omega \gg 1.
\end{cases}
$$

Proof. Both $J_0(z)$ and $z^{-1}J_1(z)$ are entire functions of z (McLachlan, 1955). Furthermore, substituting $z = 2\sqrt{-s/(2\alpha)}$ into them yields

$$J_0\left(2\sqrt{-\frac{s}{2\alpha}}\right), \quad \frac{J_1\left(2\sqrt{-\frac{s}{2\alpha}}\right)}{\sqrt{-\frac{s}{2\alpha}}} \tag{9}$$

that are entire functions as well. From the fact that G_∞ is defined as the ratio of the functions in (9), the poles and zeros of G_∞ are exactly the zeros of (9). Furthermore, all zeros of $J_0(z)$ and $z^{-1}J_1(z)$ are real-valued and simple, and the zeros and poles of them are located interchangeably on the non-negative real axis (McLachlan, 1955). Hence, considering the range of value of $2\sqrt{-s/(2\alpha)}$ proves (ii).

Next, we prove (iii). The first claim is readily verified from the direct calculation of $G_\infty(0)$. To prove the second claim, it suffices to show that

$$\lim_{r\to\infty} \frac{\alpha}{\beta}\sqrt{\frac{re^{j\theta}}{2\alpha}}G_\infty(re^{j\theta}) = 1 \tag{10}$$

holds for any θ satisfying $|\theta| < \pi$. We use the asymptotic expansion of the Bessel function (McLachlan, 1955). If $z \in \mathbb{C}$ satisfies $\left|\arg z\right| < \pi$ and $|z| \gg 1$, the Bessel function is approximated by

$$J_k(z) \sim \sqrt{\frac{2}{\pi z}}\cos\left(z - \frac{2k+1}{4}\pi\right). \tag{11}$$

Using (11), we have

$$\frac{\alpha}{\beta}\sqrt{\frac{s}{2\alpha}}G_\infty(s) \sim \frac{\sqrt{\frac{s}{2\alpha}}\cos\left(2\sqrt{-\frac{s}{2\alpha}} - \frac{3}{4}\pi\right)}{\sqrt{-\frac{s}{2\alpha}}\cos\left(2\sqrt{-\frac{s}{2\alpha}} - \frac{1}{4}\pi\right)}.$$

Define $\bar{r} := \sqrt{2r/\alpha} \geq 0$. Taking the principal value of the square roots yields

$$\sqrt{\frac{s}{2\alpha}} = \frac{\bar{r}}{2}e^{j\frac{\theta}{2}}, \quad \sqrt{-\frac{s}{2\alpha}} = \begin{cases} -j\dfrac{\bar{r}}{2}e^{j\frac{\theta}{2}}, & \theta \in (0,\pi) \\ j\dfrac{\bar{r}}{2}e^{j\frac{\theta}{2}}, & \theta \in (-\pi,0]. \end{cases}$$

Hence, (10) follows from the fact that

$$\lim_{\bar{r}\to\infty} \frac{\cos\left(-j\bar{r}e^{j\frac{\theta}{2}} - \frac{3}{4}\pi\right)}{\cos\left(-j\bar{r}e^{j\frac{\theta}{2}} - \frac{1}{4}\pi\right)}$$
$$= \lim_{\bar{r}\to\infty} \frac{e^{\bar{r}\cos\frac{\theta}{2}}e^{(\bar{r}\sin\frac{\theta}{2}-\frac{3}{4}\pi)j} + e^{-\bar{r}\cos\frac{\theta}{2}}e^{-(\bar{r}\sin\frac{\theta}{2}-\frac{3}{4}\pi)j}}{e^{\bar{r}\cos\frac{\theta}{2}}e^{(\bar{r}\sin\frac{\theta}{2}-\frac{1}{4}\pi)j} + e^{-\bar{r}\cos\frac{\theta}{2}}e^{-(\bar{r}\sin\frac{\theta}{2}-\frac{1}{4}\pi)j}} = -j$$

holds for $\theta \in (0,\pi)$, and

$$\lim_{\bar{r}\to\infty} \frac{\cos\left(j\bar{r}e^{j\frac{\theta}{2}} - \frac{3}{4}\pi\right)}{\cos\left(j\bar{r}e^{j\frac{\theta}{2}} - \frac{1}{4}\pi\right)}$$
$$= \lim_{\bar{r}\to\infty} \frac{e^{-\bar{r}\cos\frac{\theta}{2}}e^{(-\bar{r}\sin\frac{\theta}{2}-\frac{3}{4}\pi)j} + e^{\bar{r}\cos\frac{\theta}{2}}e^{-(-\bar{r}\sin\frac{\theta}{2}-\frac{3}{4}\pi)j}}{e^{-\bar{r}\cos\frac{\theta}{2}}e^{(-\bar{r}\sin\frac{\theta}{2}-\frac{1}{4}\pi)j} + e^{\bar{r}\cos\frac{\theta}{2}}e^{-(-\bar{r}\sin\frac{\theta}{2}-\frac{1}{4}\pi)j}} = j$$

holds for $\theta \in (-\pi,0]$.

From the discussion above, G_∞ is an analytic function in the right half plane. Furthermore, the boundedness of G_∞ in the right half-plane follows from (10). Hence, (i) follows. $\square$

Practical interpretation of Theorems 1 and 2 is given in Section 4.1.

4. PI Control System Design Based on Spatial Discretization

4.1. Finite-Dimensional Approximation via Spatial Discretization

We derive a finite-dimensional approximant of (3) by using a standard spatial discretization approach (Strikwerda, 2004; Takami and Kawamura, 1994). Let us approximate the continuous spatial variable $\xi \in [0,1]$ by a set of discrete points $\xi_k := k/n$ for $k \in \{0,1,\ldots,n\}$. Defining the state variables by $x_i(t) := \mathcal{X}(t,\xi_i)$ for each $i \in \{1,\ldots,n\}$, we have the state equation

$$\dot{x}_i = 2\alpha\frac{1}{\Delta\xi}\left\{\frac{\xi_i(x_{i+1} - x_i)}{\Delta\xi} - \frac{\xi_{i-1}(x_i - x_{i-1})}{\Delta\xi}\right\}$$
$$= \alpha n\{-r_{i-1}x_{i-1} + (r_{i-1} + r_i)x_i - r_i x_{i+1}\}$$

where $\Delta\xi := 1/n$ and $r_i := 2i$. Note that x_0 is replaced with 0, and x_{n+1} is replaced with the input signal $(\beta/\alpha)u$, as complying with the boundary conditions. Furthermore, the output equation is given by

$$y = \sum_{i=1}^{n} x_i\Delta\xi = \frac{1}{n}\sum_{i=1}^{n} x_i.$$

Then, we obtain a finite-dimensional state-space model as

$$\begin{cases} \dot{x} = Ax + bu \\ y = cx \end{cases}$$

where $x := [x_1,\ldots,x_n]^\mathsf{T}$ and

$$A = -\alpha n\begin{bmatrix} r_1 & -r_1 & & & \\ -r_1 & r_1 + r_2 & -r_2 & & \\ & \ddots & \ddots & \ddots & \\ & & \ddots & \ddots & -r_{n-1} \\ & & & -r_{n-1} & r_{n-1} + r_n \end{bmatrix}$$
$$b = \beta n r_n\begin{bmatrix} 0 \\ \vdots \\ 0 \\ 1 \end{bmatrix}, \quad c = n^{-1}\begin{bmatrix} 1 & \cdots & 1 \end{bmatrix}. \tag{12}$$

Hereafter, we denote its transfer function by

$$G_n(s) := c(sI_n - A)^{-1}b. \tag{13}$$

This finite-dimensional model is reasonable in the following sense: We can verify that A in (12) is rewritten as $A = -\alpha nLRL^\mathsf{T}$ with

$$L = \begin{bmatrix} 1 & & & \\ -1 & 1 & & \\ & \ddots & \ddots & \\ & & -1 & 1 \end{bmatrix}, \quad R = \begin{bmatrix} r_1 & & & \\ & r_2 & & \\ & & \ddots & \\ & & & r_n \end{bmatrix}.$$
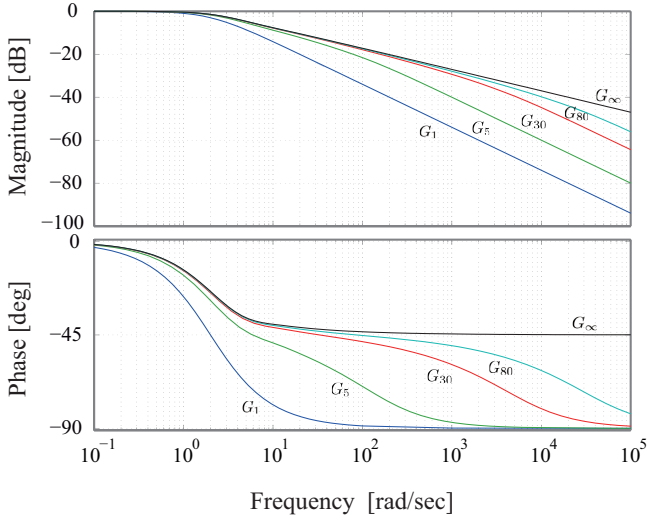
Figure 6: Bode Diagrams of the Spatial Discretization Model and the PDE System.

Figure 7: Bode Diagrams of the Spatial Discretization Model and the Machine Experiment.

This representation of A implies that it is symmetric and negative definite, namely, stable for any n. The stability of the original G_∞ is proven in Theorem 2 (i). Moreover, since the inverse of L is given by

$$L^{-1} = \begin{bmatrix} 1 & & \\ \vdots & \ddots & \\ 1 & \cdots & 1 \end{bmatrix},$$

we can verify that $G_n(0) = -cA^{-1}b = \beta/\alpha$. This implies that the steady-state value of G_n does not depend on n. Furthermore, it is identical to $G_\infty(0)$, as shown in Theorem 2 (iii).

We observe the variations of G_n with respect to n. Figure 6 depicts the Bode diagrams of G_n for $n \in \{1, 5, 30, 80\}$ and that of G_∞ in Theorem 1. This figure shows that, as n increases, the frequency property of G_n approaches that of G_∞ gradually from the low-frequency range to the high-frequency range, and the slope of the gain characteristic of G_n approaches -10 dB/dec. From this observation, we can expect that the behavior of G_n comes closer to the behavior of the PDE model in (3) as n increases. Furthermore, the property in Theorem 2 (ii) leads to the fall-off of the gain characteristics at -10 dB/dec in the high-frequency range. This property is mathematically rephrased in Theorem 2 (iii).

Next, we compare the system G_n with the molding machine. The Bode diagrams of G_1, G_{80} and the molding machine are shown in Fig. 7. The molding machine property is identified by the frequency response method. We can see from Fig. 7 that the slope of the gain characteristics of the machine is also -10 dB/dec in the high-frequency range (with the mismatch of the phase in high-frequency ranges possibly being caused by time delay from the system identification equipment). This feature conforms to the result of Theorem 2-(iii). Furthermore, Fig. 8 shows the step responses of the closed-loop system. From this figure, we can see that the step response of G_{80} properly captures that of the molding machine. Note that the poor settling
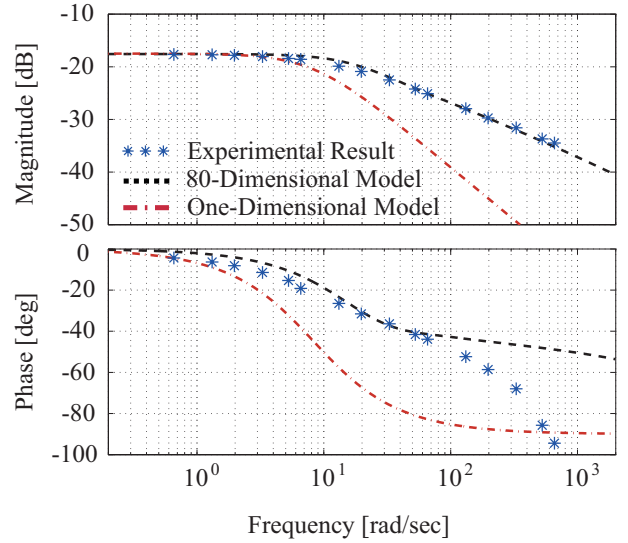
time to the steady-state value, observed in Section 2, is appropriately captured as well.

In general, the gain characteristics of rational functions having relative degree k falls off at a slope of $-20k$ dB/dec in the high-frequency range. This implies that the behavior of the molding machine is hard to capture by (especially low-dimensional) rational functions. Actually, as shown in Fig. 8, the first-order model G_1 does not follow the oscillatory behavior as well as the poor settling property. Hence, from the analyses above, we conclude that the unique behavior of the molding machine can be captured only by a high-dimensional spatial discretization model.

4.2. Finite-Frequency Loop-Shaping via Spatial Discretization

First, we introduce a PI control design method via the GKYP lemma (see Appendix A), and we then apply it to the spatially discretized model derived in Section 4.1 (Iwasaki and Hara, 2005; Hara et al., 2006). We define the open-loop transfer function L_K, which is composed of a system X and the PI controller K, by

$$L_K(s; X) := K(s)X(s), \quad K(s) := k_P + \frac{k_I}{s}. \tag{14}$$

In this notation, we consider the following loop-shaping problem:

Problem. *Given a set of transfer functions X_i, a set of non-negative real numbers $\Omega_i \subset \mathbb{R}_+$, and a set of real numbers $(a_i, b_i, c_i) \in \mathbb{R}^3$ for $i \in \{1, \ldots, m\}$, find all k_P and k_I in (14) such that*

$$a_i \mathrm{Re}[L_K(j\omega; X_i)] + b_i \mathrm{Im}[L_K(j\omega; X_i)] < c_i \tag{15}$$

for all $\omega \in \Omega_i$ and $i \in \{1, \ldots, m\}$.

6
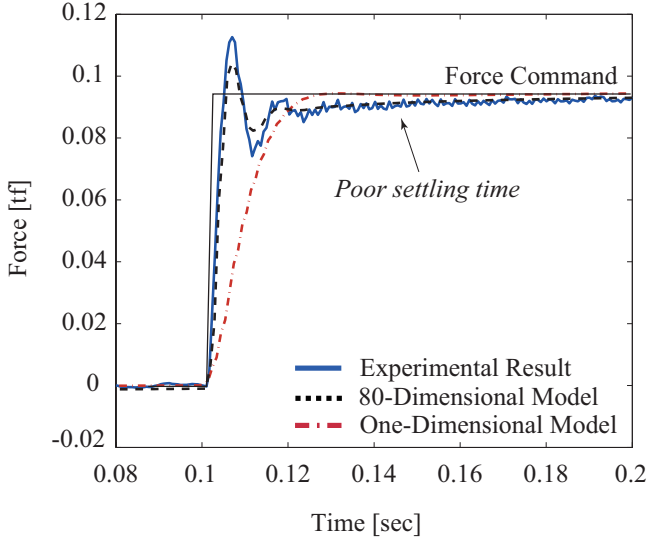
Figure 8: Step Responses of the Discretized Model and the Machine Experiment.

As shown in (15), this loop-shaping problem is formulated in terms of frequency domain inequalities. Actually, solving the problem by trial and error is a time-consuming task. Conversely, since the structure of K is restricted to the PI controllers, the GKYP lemma can equivalently translate the problem with a set of rational functions X_i into linear matrix inequalities (LMIs). In fact, LMIs can be efficiently solved especially for low-dimensional matrices.

More specifically, the frequency domain inequality (15) can be transformed to LMIs as follows: For a given rational function $X_i(s) = C_i(sI_n - A_i)^{-1}B_i$, the open-loop transfer function L_K in (15) can be represented by

$$L_K(s; X_i) = C_i(sI_{n+1} - \mathcal{A}_i)^{-1}\mathcal{B}_i$$

where

$$\mathcal{A}_i = \begin{bmatrix} 0 & C_i \\ 0 & A_i \end{bmatrix}, \quad \mathcal{B}_i = \begin{bmatrix} 0 \\ B_i \end{bmatrix}, \quad \mathcal{C}_i = \begin{bmatrix} k_I & k_P C_i \end{bmatrix}.$$

Furthermore, suppose that $\Omega_i = [\omega_1, \omega_2] \subset \mathbb{R}_+$ and $(a_i, b_i, c_i) \in \mathbb{R}^3$ are given. Then, (15) holds for all $\omega \in \Omega_i$ if and only if there exist $P_i = P_i^*$ and $Q_i = Q_i^* > 0$ such that

$$\begin{bmatrix} \mathcal{A}_i & \mathcal{B}_i \\ I_{n+1} & 0 \end{bmatrix}^* (\Phi \otimes P_i + \Psi_i \otimes Q_i) \begin{bmatrix} \mathcal{A}_i & \mathcal{B}_i \\ I_{n+1} & 0 \end{bmatrix} + \Theta_i < 0 \quad (16)$$

holds, where $\otimes$ denotes the Kronecker product and

$$\Phi = \begin{bmatrix} 0 & 1 \\ 1 & 0 \end{bmatrix}, \quad \Psi_i = \begin{bmatrix} -1 & j\dfrac{\omega_1 + \omega_2}{2} \\ -j\dfrac{\omega_1 + \omega_2}{2} & -\omega_1\omega_2 \end{bmatrix}$$

$$\Theta_i = \begin{bmatrix} C_i & 0 \\ 0 & 1 \end{bmatrix}^* \Pi_i \begin{bmatrix} C_i & 0 \\ 0 & 1 \end{bmatrix}, \quad \Pi_i = \frac{1}{2}\begin{bmatrix} 0 & a_i + jb_i \\ a_i - jb_i & 2c_i \end{bmatrix}.$$

Note that, since (16) is linear with respect to not only k_P and k_I but also c_i, we can use them as a set of LMI decision variables. Based on this LMI, we can determine a feasible gain parameter space under a given constraint.

The optimization approach to solve the loop-shaping problem is actually similar to parameter space methods; see (Saeki and Aimoto, 2000) for example. This kind of method finds a parameter space that is feasible under a constraint at a finite number of frequency points. However, it should be remarked that the satisfaction of the frequency domain inequality at a *finite* number of points is not necessarily sufficient because it is just a necessary condition to meet (15) for all $\omega \in \Omega_i$. In contrast, the GKYP lemma-based loop-shaping method can solve the loop-shaping problem with respect to an *infinite* number of frequency points by solving equivalent LMIs. The mathematical exactness is a major advantage of the GKYP lemma-based loop-shaping method. An interpretation of Ω_i and (a_i, b_i, c_i), and their relation to the design problem will be more clearly explained through the discussion that follows.

It should be further noted that this loop-shaping problem cannot be solved for the infinite-dimensional G_∞ in (4) straightforwardly, although the direct use of G_∞ is desirable. Alternatively, based on the observation in Section 4.1, we may use G_{80}, which appropriately captures the property of G_∞. However, such a high-dimensional model is not necessarily tractable. This is because heavy computational cost is required to solve the LMIs, and it is possibly time-consuming for adjusting design specifications. Furthermore, an alternative framework to capture the decay of -10 db/dec is available based on knowledge of fractional order systems (Podlubny, 1999). However, such a fractional order model is not practically implementable because the systems are inevitably infinite-dimensional.

In view of this, let us use the five-dimensional model G_5 in the following optimization. We find k_P and k_I such that κ is minimized under the constraint

$$\begin{cases} \Omega_1 = [1, 5], & (a_1, b_1, c_1) = (10, -1, 0) \\ \Omega_2 = [500, 1100], & (a_2, b_2, c_2) = (0, 1, -2) \\ \Omega_3 = [2000, 8000], & (a_3, b_3, c_3) = (-1.5, 1, \kappa) \end{cases} \quad (17)$$

on $X_i = FG_5$ for $i \in \{1, 2, 3\}$, where the characteristics of the filter in Fig. 3 are given by

$$F(s) = \left(\frac{1}{1 + \tau s}\right)^2, \quad \tau = 3.00 \times 10^{-4} \quad (18)$$

and the constants in (4) and (12) are assigned $\alpha = 1.2352$ and $\beta = 1.1621 \times 10^3$. The values of τ, α and β are determined as complying with the machine experiment.

For this optimization problem, we give an intuitive explanation as follows: We minimize κ under constraints on FG_5 in the finite frequency range Ω_i for $i \in \{1, 2, 3\}$. The constraints are defined by the half-planes assigned by the parameters (a_i, b_i, c_i) for $i \in \{1, 2, 3\}$. More specifically, the first and second constraints guarantee desired gains in the low- and middle-frequency ranges, and the third constraint maximizes the stability margin by minimizing κ. The gains in the low- and middle-frequency ranges are specified to achieve a desired transient rate of the closed-loop system. It should be noted that the design specification is determined only by (a_i, b_i, c_i) for $i \in \{1, 2, 3\}$, and thus, it can be simply adjustable by engineers and operators.
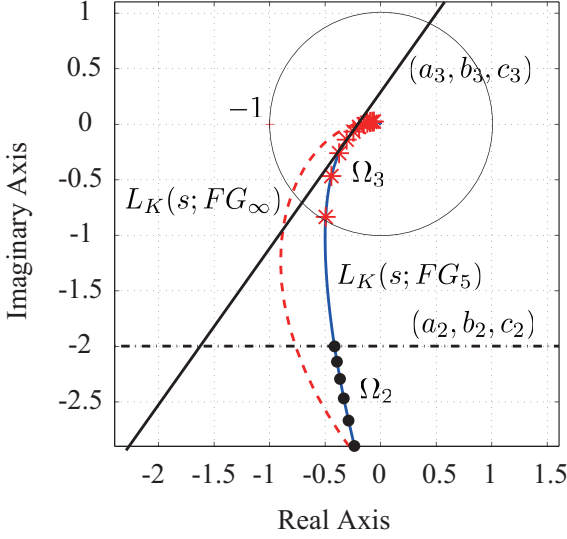
Figure 9: Nyquist Plots of Open-Loop Transfer Functions.

By solving the corresponding LMIs, we obtain the optimal solution

$$k_P = 0.0972, \quad k_I = 3.0121, \quad \kappa = 0.3283.$$

For these parameters, Fig. 9 shows the Nyquist plots of $L_K(s; FG_5)$ (solid line) and $L_K(s; FG_\infty)$ (broken line), where the lines of : and * denote the ranges of Ω_2 and Ω_3, respectively. From the Nyquist plots of $L_K(s; FG_5)$, a sufficient stability margin seems to be guaranteed. However, looking at the Nyquist plot of $L_K(s; FG_\infty)$, we see that the stability margin of the closed-loop system is severely lost. This undesirable result comes from the fact that G_5 does not capture the property of G_∞ around the high frequency range $\Omega_3 = [2000, 8000]$, in which the constraint to maximize the stability margin is imposed. This demonstrates a spillover effect caused by the unmodeled dynamics, namely the discrepancy between G_5 and G_∞.

5. PI Control System Design Based on Multiple Finite-Frequency Models

5.1. Taking Advantage of the GKYP Lemma

We propose a novel loop-shaping method based on the theoretical analysis in Section 3. In this method, the loop-shaping is performed by explicitly taking advantage of the GKYP lemma.

Recall that, in Section 4.2, we have solved the loop-shaping problem using the rational function models $X_i = FG_5$, which are identical for all $i \in \{1, 2, 3\}$ and have *real* coefficients. This setting is actually standard for control system design via the GKYP lemma; see (Hara et al., 2006) for a specific discussion on the loop-shaping problem. In contrast, our proposed loop-shaping method has the following features:

- We simultaneously use multiple different models X_i for $i \in \{1, \ldots, m\}$.

- We solve the optimization problem for rational functions having complex coefficients.

By taking advantage of these features, we execute PI gain optimization by using *different* rational transfer functions with *complex* coefficients that are valid in the specified finite frequency ranges.

As shown in Section 4.2, it is important that a finite-dimensional model appropriately captures the system properties in frequency ranges in which a set of constraints to achieve the design specification is imposed. In particular, to suppress the spillover effect degrading closed-loop stability, we require a low-dimensional model that properly captures the high-frequency properties of the system.

One possible approach for obtaining such an approximate model is to use model reduction methods. In particular, the weighted balanced truncation and the moment matching method, which approximate input-to-output characteristics for specified input signals, may be useful; see (Antoulas, 2005) for an overview for the approximation of finite-dimensional systems. However, for infinite-dimensional systems, we often face computational difficulties in constructing approximants. For example, to implement the rational interpolation method proposed in (Harkort and Deutscher, 2011), we need to solve an iterative boundary value problem for a continuous function.

In view of this difficulty, we utilize the analysis of the high-frequency characteristics of G_∞ in Theorem 2 (iii). Since the high-frequency characteristics are not expressed in terms of rational functions, we approximate it by a Taylor expansion. More specifically, denoting by $f(s; \omega_c, n)$ the n-dimensional Taylor expansion of $f(s) := (1 + \tau s)^2 \sqrt{s}$ around $s = j\omega_c$, we approximate the high-frequency property of G_∞ with the filter F by

$$F(s)G_\infty(s) \sim \frac{\beta \sqrt{2\alpha}}{\alpha} \frac{1}{f(s; \omega_c, n)} =: \hat{X}(s; \omega_c, n) \tag{19}$$

for $\omega_c \gg 1$. It should be noted that $\hat{X}$ has complex coefficients in general. Based on this approximation, we obtain a set of finite-dimensional models that are valid in the specified high-frequency ranges. In addition, we can expect that computational effort to solve LMIs will be reduced because the fine approximation is required only for the specified frequency ranges.

To ensure the validity of this approximation, we show the Bode diagrams of $\hat{X}(s; 1000, 3)$ (short-dashed line), $\hat{X}(s; 3000, 3)$ (dash dotted line) and FG_∞ (solid line) in Figure 10. From this figure, it turns out that FG_∞ is well approximated around $s = j\omega_c$ for each $\omega_c \in \{1000, 3000\}$. This observation also shows that only a three-dimensional model is sufficient for finite-frequency loop-shaping.

Using this approximate model, we find k_P and k_I such that κ is minimized under the constraint (17) on

$$X_1(s) = F(s)G_5(s), \quad X_2(s) = \hat{X}(s; 1000, 3)$$
$$X_3(s) = \hat{X}(s; 3000, 3). \tag{20}$$

Then we obtain the optimal solution

$$k_P = 0.0499, \quad k_I = 4.6150, \quad \kappa = 0.3486.$$

For these parameters, Figure 11 depicts the Nyquist plots of $L_K(s; FG_\infty)$ (solid line) and $L_K(s; X_i)$ (broken lines) for $i \in$
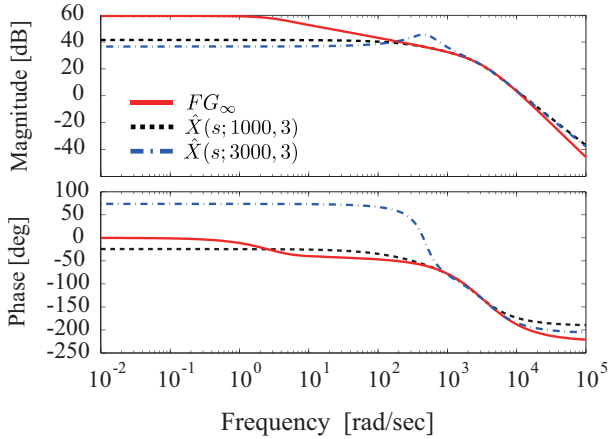
Figure 10: Approximation by Taylor Expansion.
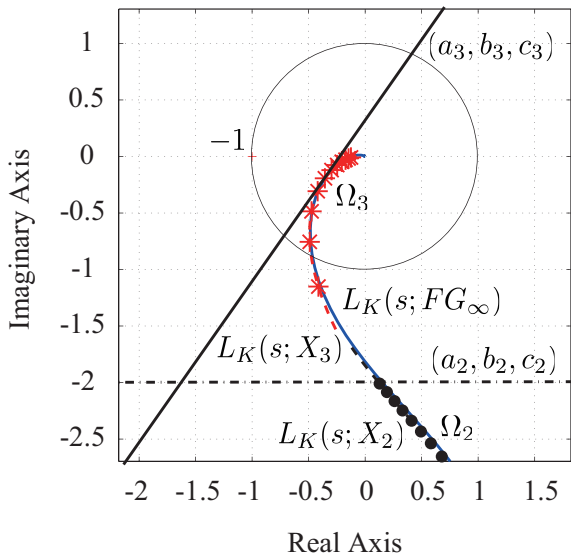
Figure 11: Nyquist Plots of Open-Loop Transfer Functions.

$\{1, 2, 3\}$, where the lines of : and $*$ denote the ranges of Ω_2 and Ω_3, respectively. This figure shows that maximization of the stability margin is successfully achieved without a large discrepancy. In fact, the spillover effect is suppressed despite the use of low-dimensional approximants. This success comes from developing a novel loop-shaping framework; that is, we use the GKYP lemma-based loop-shaping method in conjunction with a set of multiple low-dimensional approximate models that work in specified finite frequency ranges.

We summarize the procedure of the proposed method. For a given infinite-dimensional transfer function G_∞ in (4) with a filter F in (18), the GKYP lemma-based loop-shaping is carried out as follows:

(i) Determine a design specification by giving a set of frequency ranges $\Omega_i \subset \mathbb{R}_+$, and a set of half-planes described by $(a_i, b_i, c_i) \in \mathbb{R}^3$ for $i \in \{1, \dots, m\}$ in the frequency domain inequality (15).

(ii) Construct a set of rational function models $X_i(s)$, which

can be given as the Taylor expansion model $\hat{X}(s; \omega_c, n)$ in (19) or the spatial discretization model $G_n(s)$ in (13), such that the frequency property of $X_i(j\omega)$ appropriately approximates that of $F(j\omega)G_\infty(j\omega)$ in the frequency range $\omega \in \Omega_i$.

(iii) Find feasible controller parameters k_P and k_I by minimizing one of the parameters c_i using the equivalent LMIs defined as in (16).

It should be noted that this loop-shaping method may be applicable to infinite-dimensional (or high-dimensional) systems other than diffusion systems as in (3), as long as a set of suitable approximate models X_i, which possibly have complex coefficients, is available.

5.2. Experimental Verification

We show the efficacy of the proposed loop-shaping method through experimental verification. With several values of γ, which expresses the second constraint denoted by the dash dotted line in Figure 11, we find k_P and k_I such that κ is minimized under the constraint

$$\begin{cases} \Omega_1 = [1, 5], & (a_1, b_1, c_1) = (10, -1, 0) \\ \Omega_2 = [500, 1100], & (a_2, b_2, c_2) = (0, 1, -\gamma) \\ \Omega_3 = [2000, 8000], & (a_3, b_3, c_3) = (-1, 1, \kappa) \end{cases}$$

on (20). Then we obtain the optimal solutions

$$k_P = 9.6 \times 10^{-4}, \quad k_I = 7.3 \times 10^{-1}, \quad \kappa = 4.8 \times 10^{-3}$$

if $\gamma = 0.1$, and

$$k_P = 1.9 \times 10^{-3}, \quad k_I = 1.5, \quad \kappa = 9.6 \times 10^{-3}$$

if $\gamma = 0.2$. Compared with the experiment in Section 2, we notice that the optimal values of the proportional gain are smaller and the optimal values of the integral gain are larger than the controller gains that we have used for the experiment shown in Fig. 4.

For these optimal parameter sets, Figure 12 depicts numerical and experimental results of the closed-loop step response, where the numerical simulation is implemented by using G_{80} in (13). This figure shows that the step responses in both numerical and experimental results converge to the target value and also that the convergence rate improves by increasing the value of γ. However, discrepancies of the step response between the numerical and experimental results become larger with greater values of γ. Moreover, because of oscillation of the molding machine, we cannot execute the experiment if $\gamma \geq 0.3$. This oscillation might be the result of unmodeled elements such as the nonlinearity neglected in the derivation of (3).

In addition, Figure 13 shows a trade-off relation between γ and κ, namely, the degree of guaranteed gain in middle-frequency ranges and the degree of robustness of the closed-loop system. This trade-off relation implies that it is difficult to improve the convergence rate without losing some margin of stability. In other words, the proposed method substantially demonstrates a performance limitation of PI control for a class of thermal diffusion systems. It should be emphasized that such a limitation cannot be verified by using heuristic parameter tuning.

9
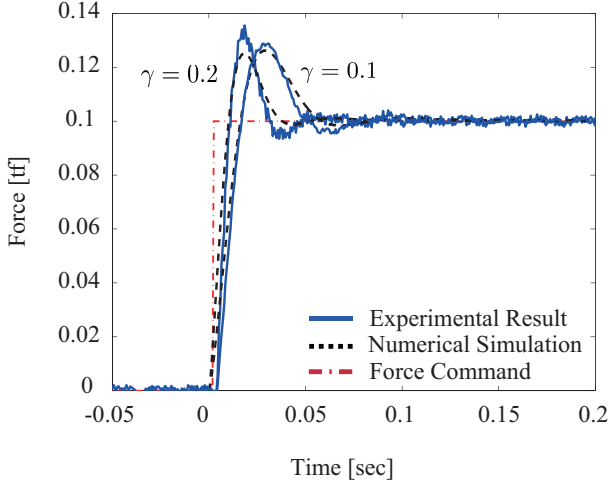
Figure 12: Numerical and Experimental Verification.
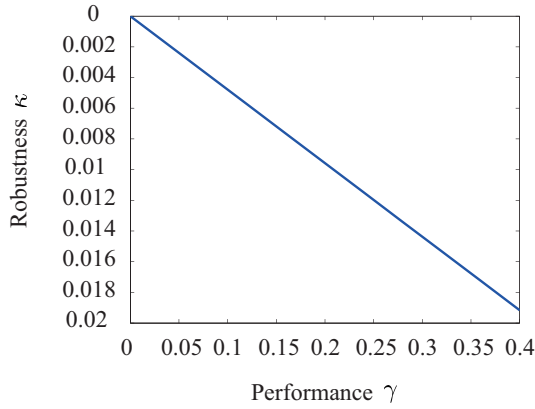
Figure 13: Trade-off Relation between κ and γ.

6. Conclusion

In this paper, we have proposed a finite-frequency loop-shaping method for an electromagnetic molding machine, which belongs to a class of infinite dimensional diffusion systems. The proposed method takes the GKYP lemma-based loop-shaping approach in conjunction with a set of multiple low-dimensional approximants that are valid in specified finite frequency ranges. By using this method, an optimization problem to design a PI control system has been solved with practical computational effort.

Spatially distributed phenomena are important to industrial applications. However, they are not necessarily tractable owing to their infinite dimensionality. One representative example is the spillover effect demonstrated in Section 4. Overcoming such a difficulty, we have solved a PI gain optimization problem for a class of infinite-dimensional systems. This success stems from the derivation of a set of finite-dimensional approximants that not only are suitable for the GKYP lemma-based loop-shaping but also appropriately capture the system property required for control system design. This result sheds light on the significance of objective-based system modelling.

Appendix A. The Generalized KYP Lemma

For reference, we provide the statement of the GKYP lemma (Iwasaki and Hara, 2005) used in this paper.

Theorem 3. *Given $A \in \mathbb{C}^{n \times n}$, $B \in \mathbb{C}^{n \times m}$, $C \in \mathbb{C}^{p \times n}$ and $D \in \mathbb{C}^{p \times m}$, define*

$$\sigma(G(\lambda), \Pi) := \begin{bmatrix} G^*(\lambda) & I_m \end{bmatrix} \Pi \begin{bmatrix} G(\lambda) \\ I_m \end{bmatrix}$$

where $\Pi = \Pi^* \in \mathbb{C}^{(p+m) \times (p+m)}$ and $G(\lambda) := C(\lambda I_n - A)^{-1} B + D$. Furthermore, define

$$\Lambda(\Phi, \Psi) := \{\lambda \in \mathbb{C} : \sigma(\lambda, \Phi) = 0, \ \sigma(\lambda, \Phi) \geq 0\},$$

where $\Phi = \Phi^* \in \mathbb{C}^{2 \times 2}$ and $\Psi = \Psi^* \in \mathbb{C}^{2 \times 2}$, and assume that $\det(\lambda I_n - A) \neq 0$ holds for all $\lambda \in \Lambda(\Phi, \Psi)$. Then, $\sigma(G(\lambda), \Pi) < 0$ holds for all $\lambda \in \Lambda(\Phi, \Psi)$ if and only if there exist $P = P^* \in \mathbb{C}^{n \times n}$ and a positive definite $Q = Q^* \in \mathbb{C}^{n \times n}$ such that

$$\begin{bmatrix} A & B \\ I_n & 0 \end{bmatrix}^* (\Phi \otimes P + \Psi \otimes Q) \begin{bmatrix} A & B \\ I_n & 0 \end{bmatrix} + \Theta < 0$$

where

$$\Theta = \begin{bmatrix} C & D \\ 0 & I_m \end{bmatrix}^* \Pi \begin{bmatrix} C & D \\ 0 & I_m \end{bmatrix}.$$

Acknowledgments

References

Antoulas, A.C., 2005. Approximation of Large-Scale Dynamical Systems. Society for Industrial Mathematics.

Astrom, K.J., Hagglund, T., 1995. PID Controllers: Theory, Design, and Tuning. ISA: The Instrumentation, Systems, and Automation Society; second edition.

Balas, M., 1978. Feedback control of flexible systems. IEEE Transactions on Automatic Control 23-4, 673–679.

Becker, R., Vexler, B., 2007. Optimal control of the convection-diffusion equation using stabilized finite element methods. Numerische Mathematik 106-3, 349–367.

Bontsema, J., Curtain, R.F., 1988. A note on spillover and robustness for flexible systems. IEEE Transactions on Automatic Control 33-6, 567–569.

Brogan, W.L., 1990. Modern Control Theory. Prentice Hall; third edition.

Calise, A.J., Prasad, J.V.R., Siciliano, B., 1990. Design of optimal output feedback compensators in two-time scale systems. IEEE Transactions on Automatic Control 35-4, 488–492.

Carslaw, H.S., Jaeger, J.C., 1986. Conduction of Heat in Solids. OXFORD SCIENCE PUBLICATIONS.

Cheng, D.K., 1992. Field and Wave Electromagnetics. Addison-Wesley; second edition.

Crank, J., 1973. The Mathematics of Diffusion. OXFORD UNIVERSITY PRESS.

Curtain, R., Morris, K., 2009. Transfer functions of distributed parameter systems: A tutorial. Automatica 45, 1101–1116.

Curtain, R., Zwart, H., 1995. An Introduction to Infinite-Dimensional Linear Systems Theory. Springer.

Deen, W.M., 1998. Analysis of Transport Phenomena. OXFORD UNIVERSITY PRESS.

DiStefano, J.J., Stubberud, A.J., Williams, I.J., 1997. Schaum's Outline of Feedback and control Systems. McGraw-Hill Professional.

Friedland, B., 2012. Control System Design: An Introduction to State-Space Methods. Courier Dover Publications.

Hara, S., Iwasaki, T., Shiokata, D., 2006. Robust PID control using generalized KYP synthesis: direct open-loop shaping in multiple frequency ranges. IEEE Control Systems Magazine 26-1, 80–91.

Harkort, C., Deutscher, J., 2011. Krylov subspace methods for linear infinite-dimensional systems. IEEE Transactions on Automatic Control 56-2, 441 – 447.

Iwasaki, T., Hara, S., 2005. Generalized KYP lemma: Unified frequency domain inequalities with design applications. IEEE Transactions on Automatic Control 50-1, 41–59.

Li, H.X., Qi, C., 2010. Modeling of distributed parameter systems for application - a synthesized review from time-space separation. Journal of Process Control 20-8, 891–901.

Li, M., Christofides, P.D., 2008. Optimal control of diffusion-convection-reaction processes using reduced-order models. Computers & Chemical Engineering 32-9, 2123–2135.

Lin, J.G., 1981. Closed-loop asymptotic stability and robustness conditions for large space systems with reduced-order controllers, in: IEEE Conference on Decision and Control including the Symposium on Adaptive Processes, pp. 1497–1502.

McLachlan, N.W., 1955. Bessel Functions for Engineers Second Edition. OXFORD UNIVERSITY PRESS.

Morita, H., Kato, A., Yamamoto, T., Shibata, T., 2009. WO publication. Technical Report. WO2009/028488.

O'Dwyer, A., 2009. Handbook of PI and PID Controller Tuning Rules. Imperial College Press; third edition.

Padhi, R., Ali, S.F., 2009. An account of chronological developments in control of distributed parameter systems. Annual Reviews in Control 33, 59–68.

Podlubny, I., 1999. Fractional-order systems and $PI^{\lambda}D^{\mu}$-controllers. IEEE Transactions on Automatic Control 44-1, 208–214.

Saeki, M., Aimoto, K., 2000. PID controller optimization for H_{∞} control by linear programming. International Journal of Robust and Nonlinear Control 10, 83–99.

Strikwerda, J., 2004. Finite Difference Schemes and Partial Differential Equations. Society for Industrial and Applied Mathematics; second edition.

Takami, H., Kawamura, T., 1994. Partial Differential Equations by the Finite Difference Method. University of Tokyo Press.

Zheng, D., Hoo, K.A., Piovoso, M.J., 2002. Finite dimensional modeling and control of distributed parameter systems, in: Proc. of American Control Conference, pp. 4377–4382.

Zhiqiang, G., Rhinehart, R.R., 2004. Theory vs. practice: the challenges from industry, in: Proc. American Control Conference, pp. 1341 – 1349.